

Many-body Majorana braiding without an exponential Hilbert space

Eric Mascot,¹ Themba Hodge,¹ Dan Crawford,¹ Jasmin Bedow,² Dirk K. Morr,² and Stephan Rachel¹

¹*School of Physics, University of Melbourne, Parkville, VIC 3010, Australia*

²*University of Illinois at Chicago, Chicago, IL 60607, USA*

(Dated: March 3, 2023)

Qubits built out of Majorana zero modes (MZMs) constitute the primary path towards topologically protected quantum computing. Simulating the braiding process of multiple MZMs corresponds to the quantum dynamics of a superconducting many-body system. It is crucial to study the Majorana dynamics both in the presence of all other quasiparticles and for reasonably large system sizes. We present a method to calculate arbitrary many-body wavefunctions as well as their expectation values and overlaps from time evolved single-particle states of a superconductor, allowing for significantly larger system sizes. We calculate the fidelity, transition probabilities, and joint parities of Majorana pairs to track the quality of the braiding process. We show how the braiding success depends on the speed of the braid. We are also able to compute arbitrary correlation functions in time and space. Our work opens the path to test and analyze the many theoretical implementations of Majorana qubits. Moreover, this method can be used to study the dynamics of any non-interacting superconductor.

Introduction.—There is hardly any physics topic which has attracted the public’s attention in the past few years more than quantum computing. With the advent of commercially available noisy intermediate-scale quantum computers, the focus has drifted towards *fault-tolerant* quantum computing architectures. Topological quantum computing might be the most exciting and fascinating strategy to accomplish fault-tolerance [1]. In a nutshell, exotic particles which obey non-Abelian braiding statistics are used to construct quantum bits (qubits). Unitary operations are realized by braiding of these anyons, and measurement is accomplished by analyzing the multi-anyon states [1, 2]. Traditionally, the prime example of a topological state hosting non-Abelian anyons has been the $\nu = 5/2$ fractional quantum Hall state [1, 3], but in the past decade topological superconductivity has proven to be a major alternative [4, 5], due to the ability to artificially engineer such systems as nanostructures [6, 7]. In topological superconductors, localized zero-energy sub-gap states can be bound to defects such as vortices or chain ends; these quasiparticles, referred to as *Majorana zero modes* (MZMs), are for practical purposes equivalent to Ising anyons [8, 9]. Today, MZMs are considered to be the most promising candidates for the building blocks of topological qubits and fault-tolerant quantum computing [2, 10].

Compared to fermions or bosons, little is known about non-Abelian anyons and Majorana zero modes in particular. While the mathematical framework is well-established [3, 11, 12], it remains unclear what challenges and obstacles to expect when embedding this framework into a physical system. In fact, already a topological qubit consisting of four Majorana zero modes constitutes a superconducting quantum many-body system (albeit non-interacting). Hence, realistic simulations are necessary in order to address all these challenges. Exact diagonalization [13–15] is most useful, but extremely

memory intense and thus limited to small system sizes. Many important contributions focus on single-particle states [16, 17] or study low-energy effective theories [18–21], while ignoring bulk states and their potential effects on the MZMs. The construction of the many-body ground state has been reported [22], but braiding requires also excited states. A promising approach is to time-evolve the quasi-particles [23–25], although simulations on large systems, including parity measurements, have yet to be demonstrated. Majorana qubit errors have been studied using the Onishi formula [26], but this is subject to the sign problem [27, 28] for general use. The covariance matrix of Ref.[29–31] constitutes an exception and seems to have the potential to overcome most obstacles, although non-Abelian braiding has not yet been demonstrated.

To simulate topological quantum computing based on MZMs requires the ability to construct (arbitrary) many-body states. To allow for sufficiently large system sizes, it is crucial to circumvent dealing with the exponentially large Hilbert space. One must be able to time-evolve these many-body states. Finally, one should be able to compute arbitrary observables from these time-evolved states.

In this Letter, we present a method—an adaption and extension of the work of Bertsch and Robledo (BR) [32, 33]—for the efficient construction of ground state and excited states from the single-particle basis. We further demonstrate the ability to time-evolve these states, compute overlaps and expectation values and arbitrary correlators for different space and time coordinates. We present benchmarking against exact diagonalization, and dynamically perform Pauli Z and Pauli X gate operations via braiding. We show how the transition probabilities of the Pauli X gate depend on speed of the braid. We then discuss Majorana-Majorana $\langle \gamma_0 \gamma_n(t) \rangle$ and particle-particle $\langle \delta n_0 \delta n_r(t) \rangle$ correlators, the latter as an example

for a four-operator correlator. Most notably, our method is applicable to the quantum dynamics of *any* superconducting many-body system.

Method.—We consider a general time-dependent Hamiltonian in the Bogoliubov-de Gennes (BdG) form,

$$\mathcal{H}(t) = \frac{1}{2} \sum_{i,j} (c_i^\dagger \ c_i) \begin{pmatrix} H_{ij}(t) & \Delta_{ij}(t) \\ \Delta_{ji}^*(t) & -H_{ij}^*(t) \end{pmatrix} \begin{pmatrix} c_j \\ c_j^\dagger \end{pmatrix}, \quad (1)$$

where c_i^\dagger (c_i) creates (annihilates) an electron with index i , which can include site, momentum, orbital, spin, etc.; $H(t)$ is the normal-state Hamiltonian matrix; and $\Delta(t)$ is the pairing matrix. The Hamiltonian matrix is Hermitian, $H = H^\dagger$, while the pairing matrix is anti-symmetric, $\Delta = -\Delta^T$. We diagonalize the Hamiltonian at time $t = 0$ with the Bogoliubov transformation,

$$\begin{pmatrix} c_i \\ c_i^\dagger \end{pmatrix} = \sum_n \begin{pmatrix} U_{in} & V_{in}^* \\ V_{in} & U_{in}^* \end{pmatrix} \begin{pmatrix} d_n \\ d_n^\dagger \end{pmatrix}, \quad (2)$$

which yields

$$\mathcal{H}(0) = \sum_n E_n \left(d_n^\dagger d_n - \frac{1}{2} \right). \quad (3)$$

We choose the energies, E_n , to be non-negative so that the quasiparticles, d_n , are excitations. With this choice, it is clear that the ground state is the vacuum of quasiparticles, which we denote $|\mathbf{0}_d\rangle$, where $d_n |\mathbf{0}_d\rangle = 0$ for all n . Such vacua are called Bogoliubov vacua.

One method to construct the Bogoliubov vacuum state is called the *product state* [34], where all quasiparticle annihilation operators are applied on the true vacuum, $|\mathbf{0}_d\rangle \propto \prod_n d_n |\mathbf{0}_c\rangle$. However, if V is singular, this procedure will annihilate the true vacuum. Alternatively, the vacuum state can be expressed as a *Thouless state*, where $|\mathbf{0}_d\rangle \propto e^{\sum_{i,j} Z_{ij} c_i^\dagger c_j^\dagger} |\mathbf{0}_c\rangle$ and $Z = (VU^{-1})^*$ [34]. If U is singular, however, the Thouless state cannot be used either. More generally, since U and V can both be singular, the vacuum state can be expressed in the canonical basis using the Bloch-Messiah decomposition [35, 36]. The Bogoliubov matrix is decomposed as $U = C\bar{U}D^\dagger$ and $V = C^*\bar{V}D^\dagger$ where C and D are unitary and

$$\bar{U} = \begin{pmatrix} I & \\ & \oplus_k u_k \sigma_0 & \\ & & 0 \end{pmatrix}, \quad \bar{V} = \begin{pmatrix} 0 & \\ & \oplus_k v_k i \sigma_y & \\ & & I \end{pmatrix}, \quad (4)$$

with u_k, v_k positive and $u_k^2 + v_k^2 = 1$. The three blocks are called fully empty, paired, and fully occupied, corresponding to the zero, middle, and identity blocks of \bar{V} (identity, middle, and zero blocks of \bar{U}), respectively. We define new operators

$$c_i = \sum_j C_{ij} \bar{c}_j, \quad d_i = \sum_j D_{ij} \bar{d}_j, \quad (5)$$

which transform as

$$\begin{pmatrix} \bar{c}_i \\ \bar{c}_i^\dagger \end{pmatrix} = \sum_n \begin{pmatrix} \bar{U}_{in} & \bar{V}_{in} \\ \bar{V}_{in} & \bar{U}_{in} \end{pmatrix} \begin{pmatrix} \bar{d}_n \\ \bar{d}_n^\dagger \end{pmatrix}. \quad (6)$$

The d and \bar{d} quasiparticles share the same vacuum, which follows directly from Eq. (5). We construct the product state using the \bar{d} quasiparticles, truncating the fully empty modes:

$$|\mathbf{0}_d\rangle = \frac{1}{\sqrt{\mathcal{N}}} \prod_{k \in P} \bar{d}_k \bar{d}_{\bar{k}} \prod_{k \in O} \bar{d}_k |\mathbf{0}_c\rangle \quad (7)$$

$$= \prod_{k \in P} (u_k + v_k \bar{c}_k^\dagger \bar{c}_{\bar{k}}^\dagger) \prod_{k \in O} \bar{c}_k^\dagger |\mathbf{0}_c\rangle. \quad (8)$$

O denotes the fully occupied modes and P denotes the paired modes. The index, $k \in P$, iterates over paired indices, (k, \bar{k}) , corresponding to the 2×2 blocks of \bar{V} . The normalization is $\mathcal{N} = \prod_{k \in P} v_k^2$.

To construct excited states, we add excitations to the vacuum,

$$|\mathbf{n}_d\rangle = \prod_k (d_k^\dagger)^{n_k} |\mathbf{0}_d\rangle, \quad (9)$$

where $n_k \in \{0, 1\}$ is the occupation of the k -th mode. We then time-evolve the state with the time-evolution operator,

$$\mathcal{S}(t) = \mathcal{T} \exp \left(-\frac{i}{\hbar} \int_0^t dt' \mathcal{H}(t') \right), \quad (10)$$

where \mathcal{T} time-orders the integral. The time-evolved state is given by

$$|\mathbf{n}_d(t)\rangle = \prod_k (d_k^\dagger(t))^{n_k} |\mathbf{0}_d(t)\rangle, \quad (11)$$

where $d_k^\dagger(t) = \mathcal{S}(t) d_k^\dagger \mathcal{S}^{-1}(t)$ and $|\mathbf{0}_d(t)\rangle$ is the vacuum of time-evolved quasiparticles, $d(t)$. The time-evolved Bogoliubov vacuum can be obtained by directly time-evolving the state. However, it is convenient to construct the Bogoliubov vacuum from the time-evolved quasiparticles. Since these represent the same state, they must be related by a phase. For most observables, this phase drops out. We show the explicit calculation for this phase in the supplemental material [37].

Time-evolving the operators is done using the time-dependent BdG equations [16, 23–26],

$$i\hbar \frac{\partial}{\partial t} \begin{pmatrix} U(t) & V^*(t) \\ V(t) & U^*(t) \end{pmatrix} = H_{\text{BdG}}(t) \begin{pmatrix} U(t) & V^*(t) \\ V(t) & U^*(t) \end{pmatrix}, \quad (12)$$

where $H_{\text{BdG}}(t)$ is the matrix in Eq. (1) and the initial conditions are given by the Bogoliubov transformation in Eq. (2). The time-evolved quasiparticles are given by

$$\begin{pmatrix} c_i \\ c_i^\dagger \end{pmatrix} = \sum_n \begin{pmatrix} U_{in}(t) & V_{in}^*(t) \\ V_{in}(t) & U_{in}^*(t) \end{pmatrix} \begin{pmatrix} d_n(t) \\ d_n^\dagger(t) \end{pmatrix}. \quad (13)$$

The time-evolved Bogoliubov vacuum is then given by

$$|\mathbf{0}_d(t)\rangle = \frac{e^{i\alpha(t)}}{\sqrt{\mathcal{N}(t)}} \prod_{k \in P} \bar{d}_k(t) \bar{d}_{\bar{k}}(t) \prod_{k \in O} \bar{d}_k(t) |\mathbf{0}_c\rangle, \quad (14)$$

where $d_i(t) = \sum_j D_{ij}(t) \bar{d}_j(t)$ and $\mathcal{N}(t) = \prod_{k \in P} v_k^2(t)$, using the time-dependent Bloch-Messiah decomposition $U(t) = C(t) \bar{U}(t) D^\dagger(t)$ and $V(t) = C^*(t) \bar{V}(t) D^\dagger(t)$. The

phase $\alpha(t)$ is the phase difference between the time-evolved Bogoliubov vacuum and the product state of time-evolved quasiparticles.

Consider the quantity $\langle \mathbf{n}_d(t) | \mathcal{A} | \mathbf{n}'_d(t') \rangle$ where \mathcal{A} is an arbitrary product of creation and annihilation operators. For example, to calculate overlaps between states, we set $\mathcal{A} = 1$, or to calculate expectation values, we set $|\mathbf{n}'_d(t')\rangle = |\mathbf{n}_d(t)\rangle$. By adapting a formula by Bertsch and Robledo [32, 33, 36], this quantity becomes a Pfaffian:

$$\langle \mathbf{n}_d(t) | \mathcal{A} | \mathbf{n}'_d(t') \rangle = \pm \frac{e^{-i(\alpha(t) - \alpha(t'))}}{\sqrt{\mathcal{N}(t)\mathcal{N}(t')}} \text{pf} \begin{pmatrix} \overline{d^\dagger(t)\bar{d}^\dagger(t)} & \overline{d^\dagger(t)d(t)} & \overline{d^\dagger(t)\mathcal{A}} & \overline{d^\dagger(t)d^\dagger(t')} & \overline{d^\dagger(t)\bar{d}(t')} \\ \overline{d(t)\bar{d}(t)} & \overline{d(t)\mathcal{A}} & \overline{d(t)d^\dagger(t')} & \overline{d(t)\bar{d}(t')} & \\ \overline{\mathcal{A}\mathcal{A}} & \overline{\mathcal{A}d^\dagger(t')} & \overline{\mathcal{A}\bar{d}(t')} & & \\ \overline{d^\dagger(t')d^\dagger(t')} & \overline{\mathcal{A}d(t')} & \overline{\mathcal{A}\bar{d}(t')} & & \\ & \overline{\bar{d}(t')\bar{d}(t')} & & & \end{pmatrix}. \quad (15)$$

The lower triangle is obtained by anti-symmetry. The sign is derived from reversing the order of operators in $\langle \mathbf{n}_d(t) |$ and is given by $\pm = (-1)^{n_{\bar{d}}(n_{\bar{d}}-1)/2 + n_d(n_d-1)/2}$ where $n_{\bar{d}}(n_d)$ is the number of $\bar{d}^\dagger(t)$ ($d(t)$) operators in $\langle \mathbf{n}_d(t) |$. ab denotes the matrix of contractions such that $[ab]_{ij} = \langle \mathbf{0}_c | a_i b_j | \mathbf{0}_c \rangle$. This matrix only includes occupied modes and rows/columns of unoccupied modes are truncated. We list useful contraction matrices in Table I. In the following, we will refer to the methodology used in this paper simply as the Bertsch–Robledo (BR) method.

Results.—For the remainder of the paper, we use the Kitaev chain [5] as the standard model of a topological superconductor (TSC) hosting Majorana zero modes. It represents the low-energy theory of essentially all 1D TSC models, i.e., we do not need to specify the physical system but our results are relevant for all Majorana platforms. The Kitaev chain is given by Eq. (1) with $H_{ij} = -\mu_i(t)\delta_{ij} - \tilde{t}(\delta_{i,j+1} + \delta_{i+1,j})$ and $\Delta_{ij} = e^{i\phi} |\Delta_p| (\delta_{ij+1} - \delta_{j+1,i})$, where μ, \tilde{t}, Δ_p and ϕ correspond to the chemical potential, tunneling strength, p -wave pairing strength and its phase, respectively. Throughout the paper we set $\tilde{t} = \Delta_p$; for details see the supplemental material [37]. The topological phase with MZMs at chain ends is realized for $-2\tilde{t} < \mu_{\text{topo}} < 2\tilde{t}$ [5]. The total braiding time is denoted as T , and the delay coefficient α is the relative time between the ramping protocol of two neighboring sites. That is, $\alpha = 0$ means that $\mu_i(t)$ of all sites on a given leg are changed simultaneously, while for $\alpha = 1$ only $\mu_i(t)$ of a single site is changed at once.

Benchmarking: Bertsch-Robledo vs. Exact Diagonalization.—Our first result is the demonstration of a Pauli Z gate on a T-junction with leg length $L = 5$, corresponding to a total number of sites $N = 16$.

The Kitaev chain model is modified straight-forwardly to fit onto the T-junction so that all pairing phases on the horizontal (vertical) legs are $\phi = 0$ ($\phi = \pi/2$), corresponding to a $p_x + ip_y$ superconductor. Moreover, the central site connects to all three legs via hoppings and pairings [37]. We have chosen a rather small system size in order to allow comparison between the BR method and the full many-body states. Time-evolution is simulated by approximating the time-evolution opera-

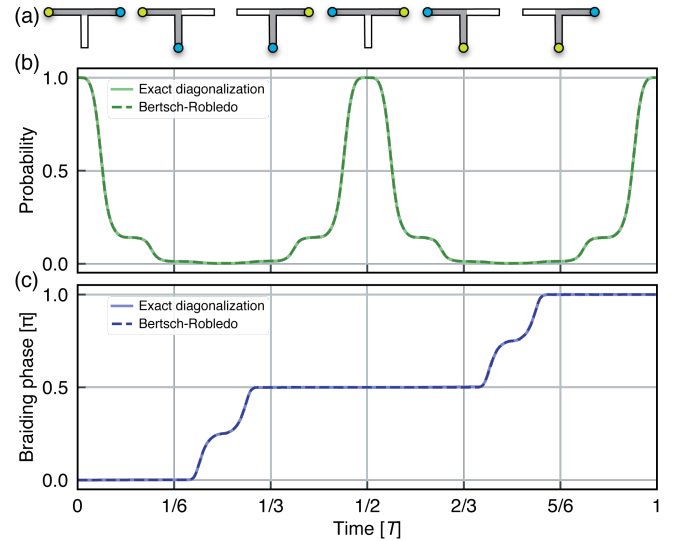


FIG. 1. Z gate on a T-junction ($L = 5$). (a) Steps to perform braid. (b) Probability $|\langle 1|1(t)\rangle|^2$ using both exact diagonalization and BR method. (c) Geometric phase using both methods. Parameters: $(\mu_{\text{topo}}, \mu_{\text{triv}}, \alpha, T) = (-0.05\tilde{t}, -4\tilde{t}, 0.025, 960\hbar/\tilde{t})$.

TABLE I. Contraction matrices, $M_{ij} = \langle \mathbf{0}_c | a_i b_j | \mathbf{0}_c \rangle$, between a (row) and b (column).

	$d^\dagger(t')$	$d(t')$	$\bar{d}^\dagger(t')$	$\bar{d}(t')$
$d(t)$	$U^\dagger(t)U(t')$	$U^\dagger(t)V^*(t')$	$U^\dagger(t)C(t')\bar{U}(t')$	$U^\dagger(t)C(t')\bar{V}(t')$
$d^\dagger(t)$	$V^T(t)U(t')$	$V^T(t)V^*(t')$	$V^T(t)C(t')\bar{U}(t')$	$V^T(t)C(t')\bar{V}(t')$
$\bar{d}(t)$	$\bar{U}(t)C^\dagger(t)U(t')$	$\bar{U}(t)C^\dagger(t)V^*(t')$	$\bar{U}(t)C^\dagger(t)C(t')\bar{U}(t')$	$\bar{U}(t)C^\dagger(t)C(t')\bar{V}(t')$
$\bar{d}^\dagger(t)$	$\bar{V}^T(t)C^\dagger(t)U(t')$	$\bar{V}^T(t)C^\dagger(t)V^*(t')$	$\bar{V}^T(t)C^\dagger(t)C(t')\bar{U}(t')$	$\bar{V}^T(t)C^\dagger(t)C(t')\bar{V}(t')$

tor as $\exp(-iH\delta t)$, which we compute using the Krylov subspace method [38, 39] for both exact diagonalization and BR method. In subsequent sections we simulate time-evolution using a more accurate 4th order implicit Runge-Kutta method [37].

The Z gate on the T-junction is realized by *moving* the Majorana modes via dynamical manipulation of the local chemical potential $\mu_i(t)$, as schematically illustrated in Fig. 1 a [40]. For details of the ramping protocol see the supplemental material [37]. To guarantee the adiabaticity of the dynamics we consider the fidelities [41] of the two degenerate many-body ground states $|0\rangle$ and $|1\rangle$. The former (latter) corresponds to the even (odd) parity sector, and they share the relationship $|1\rangle = d^\dagger|0\rangle$, where for $\mu = 0$ we simply have $d^\dagger = \frac{1}{2}(\gamma_1 + i\gamma_2 N)$.

Fig. 1 b shows the squared fidelity or probability, $|\langle 1|1(t)\rangle|^2$, which is identical to $|\langle 0|0(t)\rangle|^2$ (not shown). A fidelity is insensitive to the phase, so midway through the braid the fidelity returns to 1 even though the MZMs have been exchanged. That the states $|1\rangle$ and $|1(T/2)\rangle$ are nevertheless different is revealed through the geometric phase [13, 42] in its gauge- and parametrization-invariant form $\phi_g = \arg \langle \psi | \psi(T) \rangle - \text{Im} \int_0^T \langle \psi(t) | \dot{\psi}(t) \rangle dt$. The braiding phase, or the difference of geometric phases between odd and even parity states, is shown in Fig. 1 c: After exchanging the MZMs once, a phase $\pi/2$ is accumulated, demonstrating the anyonic character of the MZMs and their fractional statistics, while realizing a \sqrt{Z} gate. After exchanging the MZMs once more, the MZMs return to their original position and the total braiding phase π is reached, concluding the Z gate. Also, the fidelities have returned to 1, and thus there were no transitions into excited states. Note that it is not possible to perform non-Abelian statistics with only two MZMs, at least four are required (see below). The many-body calculation of a Z gate can be found in the literature [13]; here we only show it to highlight the agreement between exact diagonalization (solid lines) and the BR method (dashed lines) in Fig. 1 b and c.

The X gate and non-Abelian braiding.—Realizing M qubits requires $2M + 2$ MZMs. In the following we focus on a single qubit (i.e., four MZMs) and perform a Pauli X gate, also known as a “qubit flip”. Fig. 2 a illustrates the setup of two topological Kitaev chains with its MZMs on the T-junction; the X gate corresponds to exchanging the two inner MZMs twice. The leg length

of the T-junction is $L = 20$ sites leading to the total system size $N = 61$. In Fig. 2 b we show the transition probabilities from one ground state $|n\rangle$ into the other one $|m\rangle$, $|\langle n|m(t)\rangle|^2$, and the ground state parities in Fig. 2 c. These ground states are either $|00\rangle$ and $|11\rangle$ (total parity = even) or $|10\rangle$ and $|01\rangle$ (total parity = odd) [37]. At $t = 0$, same-state probabilities are at unity and transition probabilities at zero. Midway through the braid, all

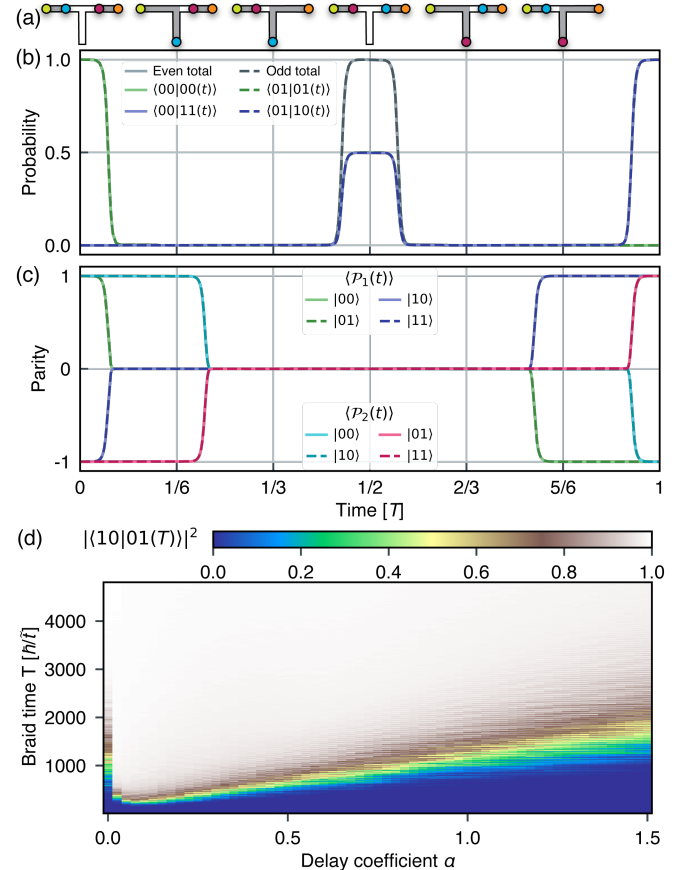


FIG. 2. X gate on a T-junction ($L = 20$). (a) Steps to perform braid. (b) Transition probabilities. Green corresponds to same state transitions, with blue corresponding to different state transitions within a parity subspace. (c) Corresponds to the first and second excited state parity calculations, calculated on all states in the even and odd parity subspaces of the Majorana sector. (d) Transition probability $|\langle 10|01(T)\rangle|^2$ as a function of braid time T and delay coefficient α . Parameters: $(\mu_{\text{topo}}, \mu_{\text{triv}}, \alpha, T) = (0.05\tilde{t}, 10\tilde{t}, 0.025, 15072\hbar/\tilde{t})$.

transition probabilities reach 1/2 signifying that each initial state has transitioned to an equal superposition with the other initial state (corresponding to a \sqrt{X} gate), e.g. $|00\rangle \rightarrow e^{i\frac{\pi}{4}} (|00\rangle - i|11\rangle)/\sqrt{2}$. Their total probability adds up to 1 indicating adiabaticity. Upon completion of the braid, the transition probability reaches 1 while the same-state probability goes to 0. We have successfully switched the Majorana qubit.

Our formalism allows to compute and track another most useful quantity: the time-dependent parities of the original pairs of MZMs, i.e., of the two topological Kitaev chains, \mathcal{P}_1 and \mathcal{P}_2 with $\mathcal{P}_i = 1 - 2d_i^\dagger d_i$ and $\langle \mathcal{P}_i(t) \rangle = \langle \mathbf{n}(t) | \mathcal{P}_i | \mathbf{n}(t) \rangle$. The total parity $\mathcal{P}_{\text{tot}} = \langle \mathcal{P}_1(t) \rangle \langle \mathcal{P}_2(t) \rangle$ remains unchanged after the braid, but $\langle \mathcal{P}_1(t) \rangle$ and $\langle \mathcal{P}_2(t) \rangle$ will have swapped their initial values at the end of the braid. All eight combinations out of the two parity operators and the four ground states $\{|00\rangle, |11\rangle, |10\rangle, |01\rangle\}$ are shown in Fig. 2c. The results confirm the transition probabilities of Fig. 2b. During the first step of the braid, one Majorana in the left chain is moved down the T-junction. As the left MZM loses a Majorana, the occupation becomes 1/2 and the parity goes to zero. The drop in the parity happens simultaneously with the drop in probability, as the initial and time-evolved MZM states no longer overlap. The parity of the right MZM remains constant in the first step since the MZM stays still. Once the Majorana starts moving, then the parity begins to drop to zero. Halfway through the braid, the state is an equal superposition of occupied and unoccupied, so the expectation value of the parity remains at zero. When the Majorana returns to its original position, the parity finally becomes non-zero, and is opposite to the initial value.

Fig. 2b also shows the total probabilities, e.g. $|\langle 00|00(t) \rangle|^2 + |\langle 00|11(t) \rangle|^2$ in case of the even parity sector; at $t = 0, T/2, T$ they reach unity, indicating the adiabaticity of the braid, i.e., absence of transitions into excited states. That raises the question about robustness of such a braid upon varying braid time T and delay coefficient α . In Fig. 2d we present $|\langle 10|01(t) \rangle|^2$ as a function of T and α . Somewhat surprisingly, for rather short braid times of $T = 1000\hbar/\tilde{t}$ or $2000\hbar/\tilde{t}$, the probability reaches already unity. Most remarkably, even at zero delay ($\alpha = 0$), i.e., when the $\mu_i(t)$ are changed simultaneously for the entire leg, by slightly increasing T , even in this extreme case we find perfect transition probabilities. Assuming a hopping amplitude of the order of 0.1 eV, we obtain e.g. a braid time $T = 1000\hbar/\tilde{t} = 6.6$ ps.

The X gate on a substrate.—The T-junction considered so far, consist of purely 1D wires and the two-dimensionality is ensured by adjusting the phase ϕ of the superconducting order parameter for the vertical and horizontal legs appropriately [13, 40]. Our approach allows us to deal with significantly larger system sizes, and we can thus extend our geometry to truly 2D. To this end, we consider a rectangular geometry of size 37×21

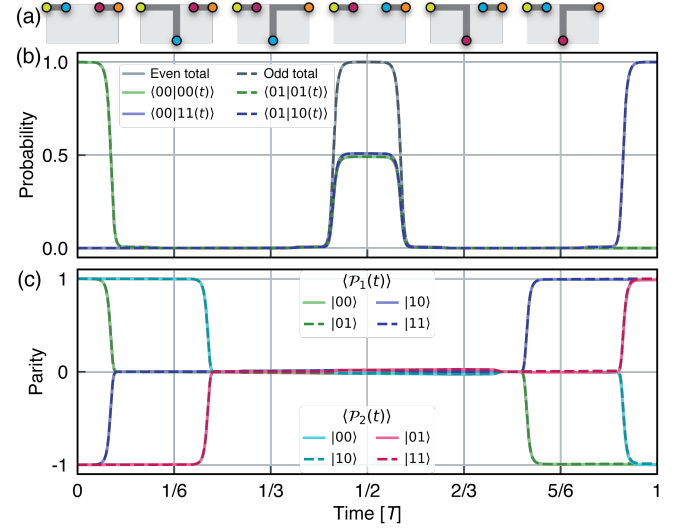


FIG. 3. X gate on a T-junction ($L = 16$) with a substrate (37×21 lattice sites). (a) Steps to perform braid. (b) Transition probabilities. (c) Parity for the degenerate ground states, in the even and odd subspaces. Parameters: $(\mu_{\text{topo}}, \mu_{\text{triv}}, \alpha, T) = (0.05\tilde{t}, 10\tilde{t}, 0.025, 12288\hbar/\tilde{t})$.

lattice sites (corresponding to $N = 777$). The chemical potential μ_{triv} is tuned to be in the trivial gapped regime everywhere, except for the topological segments of the T-junction (leg length $L = 16$) where we use μ_{topo} instead. We keep two additional trivial sites around the junction.

We perform the identical braiding dynamics as discussed in the previous part. The transition probabilities $|\langle n|m(t) \rangle|^2$ and the squared fidelities $|\langle n|n(t) \rangle|^2$ are shown in Fig. 3b, and the parities in Fig. 3c, in analogy to Fig. 2. During the braid, all features are essentially identical to the case without substrate. Most importantly, at the end of the braid ($t = T$) probabilities and parities are identical to those shown in Fig. 3. The two-dimensionality leads to comparable results for our Majorana qubit and does not constitute an obstacle.

Correlators in space and time.—The BR method enables us to compute arbitrary correlation functions. “Arbitrary” refers to m involved operators evaluated at arbitrary and different positions and times $r(t)$ and $r'(t')$. For the sake of a clear presentation, we restrict the following discussion to simple examples on a chain geometry with open boundary conditions, highlighting the potential of the method nevertheless.

As a representative and meaningful example we first show the correlations of number fluctuations $\langle \delta n_0 \delta n_r(t) \rangle$ in Fig. 4a, with $\delta n_r(t) = n_r(t) - \langle n_r(t) \rangle$. The appearance of a *light cone* is clearly visible; when it hits the boundary, the correlations reflect and can interfere with each other. These correlations are not affected by the MZMs, and we would obtain very similar results for periodic boundary conditions where the MZMs are absent entirely.

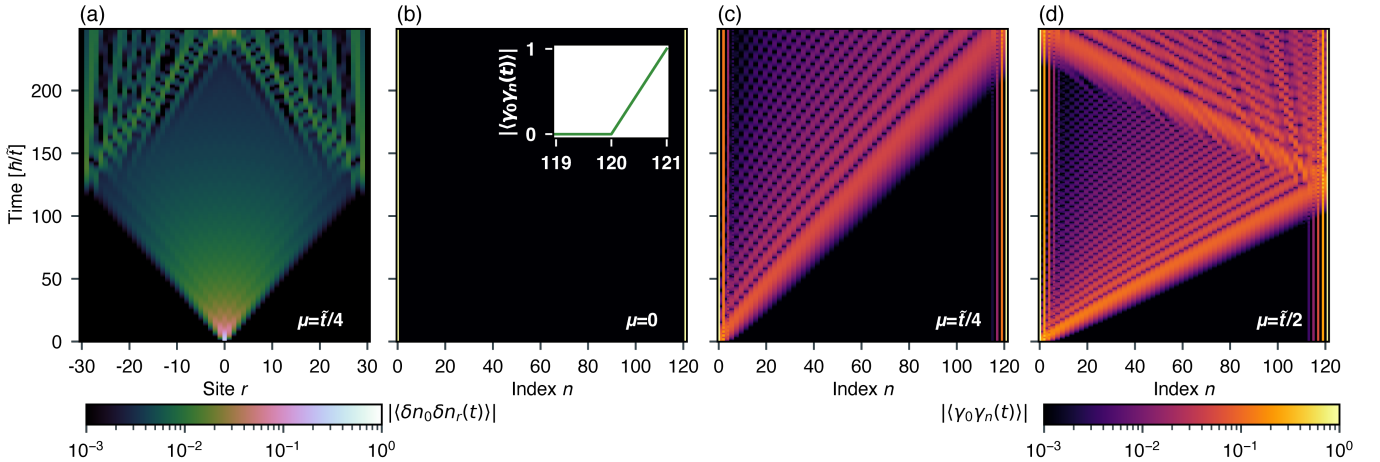


FIG. 4. (a) r - t -plane of the particle-particle correlator $\langle \delta n_0(0) \delta n_r(t) \rangle$ for an $L = 61$ chain with open boundary conditions at $\mu = 0.25\tilde{t}$. (b-d) n - t -plane where each lattice site r maps onto two Majorana indices n , thus $n_{\max} = 2L = 122$. (b) Majorana-Majorana correlator $\langle \gamma_0(0) \gamma_{23}(t) \rangle$ for the topological regime at the dimerised limit ($\mu = 0$). Note the high weight (in yellow) at $n = 0$ and $n = 121$. Inset shows the last three ‘‘Majorana sites’’ emphasizing that the Majorana bound state is strictly localized at the outer-most sites. (c) and (d) present the same correlation at $\mu = 0.25\tilde{t}$ and $\mu = 0.5\tilde{t}$, respectively.

Next we focus on correlations of the Majorana operator, $\langle \gamma_0 \gamma_n(t) \rangle$. In the topological regime of the Kitaev chain, the MZM on the left boundary should reveal long-range correlations with the one on the right boundary. This can clearly be seen in Fig. 4 b-d. Panel b shows the localized limit $\mu = 0$ where the only non-zero correlations are between the first and the last Majorana operator. That the correlations are unity at the first and last site and zero otherwise is expected; more interestingly, these results remain unchanged when time-evolving the ground state. Panel (c) and (d) show the analog cases for $\mu = \tilde{t}/4$ and $\tilde{t}/2$, respectively. We observe a finite penetration of the Majorana correlations at the edges (which is time-independent) due to the broadening of the MZM wavefunctions. In addition, we observe an additional signal reminiscent of a light cone (‘‘operator spread’’), evolving from the left edge into the system over time. This is attributed to the presence of hoppings between all Majorana operators for finite μ , and the ‘‘velocity of this cone’’ grows with increasing μ . The results of panel c and d combine the features of panels a and b, the light-cone stemming from a quasi-particle spreading over time, and the time-independent long-range correlations of the Majoranas at the edge of the chain.

This discussion could be extended to other correlators and to ramping and quenching in a straight-forward manner; it is, however, beyond the scope of this Letter and left for future work.

Outlook.—The methodological progress reported in this Letter allows one to study the dynamics of an arbitrary superconducting many-body system. Braiding of multiple qubits could be investigated. More importantly, the real-world problems of multi-Majorana systems under non-equilibrium conditions can be analyzed,

as demonstrated here for Pauli Z and X gates, representing a crucial step towards any future topological quantum computer. By choosing a Majorana platform, one can obtain specific results, such as the braiding dynamics in magnet-superconductor hybrid systems [43]. Material parameters can be included to make predictions for future experiments more reliable. With other words, this is a powerful tool to perform numerical experiments, long before the real experiments are in reach.

We acknowledge discussions with Hong-Hao Tu, B. G. Carlsson and J. Rotureau. S.R. acknowledges support from the Australian Research Council through Grant No. DP200101118. J.B. and D.K.M. acknowledge support by the U. S. Department of Energy, Office of Science, Basic Energy Sciences, under Award No. DE-FG02-05ER46225.

- [1] C. Nayak, S. H. Simon, A. Stern, M. Freedman, and S. Das Sarma, Rev. Mod. Phys. **80**, 1083 (2008).
- [2] V. Lahtinen and J. K. Pachos, SciPost Phys. **3**, 021 (2017).
- [3] G. Moore and N. Read, Nucl. Phys. B **360**, 362 (1991).
- [4] N. Read and D. Green, Phys. Rev. B **61**, 10267 (2000).
- [5] A. Y. Kitaev, Phys.-Usp. **44**, 131 (2001).
- [6] R. M. Lutchyn, J. D. Sau, and S. Das Sarma, Phys. Rev. Lett. **105**, 077001 (2010).
- [7] Y. Oreg, G. Refael, and F. von Oppen, Phys. Rev. Lett. **105**, 177002 (2010).
- [8] M. Barkeshli, C.-M. Jian, and X.-L. Qi, Phys. Rev. B **87**, 045130 (2013).
- [9] Majorana zero modes possess R matrices which are only projectively equivalent to those of Ising anyons.
- [10] C. W. J. Beenakker, SciPost Phys. Lect. Notes , 15 (2020).
- [11] E. Witten, Comm. Math. Phys. **121**, 351 (1989).

- [12] M. H. Freedman, A. Kitaev, M. J. Larsen, and Z. Wang, Bull. Amer. Math. Soc. **40**, 31 (2003).
- [13] M. Sekania, S. Plugge, M. Greiter, R. Thomale, and P. Schmitteckert, Phys. Rev. B **96**, 094307 (2017).
- [14] J. Li, T. Neupert, B. A. Bernevig, and A. Yazdani, Nat. Commun. **7**, 10395 (2016).
- [15] A. Wieckowski, M. Mierzejewski, and M. Kupczynski, Phys. Rev. B **101**, 014504 (2020).
- [16] C. S. Amorim, K. Ebihara, A. Yamakage, Y. Tanaka, and M. Sato, Phys. Rev. B **91**, 174305 (2015).
- [17] C. Tutschku, R. W. Reinthalter, C. Lei, A. H. MacDonald, and E. M. Hankiewicz, Phys. Rev. B **102**, 125407 (2020).
- [18] T. Karzig, G. Refael, and F. von Oppen, Phys. Rev. X **3**, 041017 (2013).
- [19] W. Chen, J. Wang, Y. Wu, J. Qi, J. Liu, and X. C. Xie, Phys. Rev. B **105**, 054507 (2022).
- [20] T. Karzig, F. Pientka, G. Refael, and F. von Oppen, Phys. Rev. B **91**, 201102 (2015).
- [21] C. Knapp, M. Zaletel, D. E. Liu, M. Cheng, P. Bonderup, and C. Nayak, Phys. Rev. X **6**, 041003 (2016).
- [22] B. P. Truong, K. Agarwal, and T. Pereg-Barnea, “Optimizing Transport of Majorana Zero Modes in One-Dimensional Topological Superconductors,” arXiv:2211.13849.
- [23] M. Cheng, V. Galitski, and S. Das Sarma, Phys. Rev. B **84**, 104529 (2011).
- [24] M. S. Scheurer and A. Shnirman, Phys. Rev. B **88**, 064515 (2013).
- [25] T. Sanno, S. Miyazaki, T. Mizushima, and S. Fujimoto, Phys. Rev. B **103**, 054504 (2021).
- [26] A. Conlon, D. Pellegrino, J. K. Slingerland, S. Dooley, and G. Kells, Phys. Rev. B **100**, 134307 (2019).
- [27] T. Mizusaki, M. Oi, and N. Shimizu, Phys. Lett. B **779**, 237 (2018).
- [28] L. M. Robledo, Phys. Rev. C **79**, 021302 (2009).
- [29] S. Bravyi and R. König, Commun. Math. Phys. **316**, 641 (2012).
- [30] S. Bravyi and D. Gosset, Commun. Math. Phys. **356**, 451 (2017).
- [31] B. Bauer, T. Karzig, R. V. Mishmash, A. E. Antipov, and J. Alicea, SciPost Phys. **5**, 004 (2018).
- [32] G. F. Bertsch and L. M. Robledo, Phys. Rev. Lett. **108**, 042505 (2012).
- [33] B. G. Carlsson and J. Rotureau, Phys. Rev. Lett. **126**, 172501 (2021).
- [34] H. Shi and S. Zhang, Phys. Rev. B **95**, 045144 (2017).
- [35] C. Bloch and A. Messiah, Nucl. Phys. **39**, 95 (1962).
- [36] H.-K. Jin, R.-Y. Sun, Y. Zhou, and H.-H. Tu, Phys. Rev. B **105**, L081101 (2022).
- [37] Supplemental Material.
- [38] Y. Saad, SIAM J. on Numer. Anal. **29** (1992), 10.1137/0729014.
- [39] M. Hochbruck and C. Lubich, SIAM J. Numer. Anal. **34**, 1911 (1997).
- [40] J. Alicea, Y. Oreg, G. Refael, F. von Oppen, and M. P. A. Fisher, Nat. Phys. **7**, 412 (2011).
- [41] M. A. Nielsen and I. L. Chuang, *Quantum Computation and Quantum Information* (Cambridge University Press, UK, 2000).
- [42] N. Mukunda and R. Simon, Ann. Phys. **228**, 205 (1993).
- [43] J. Bedow, E. Mascot, T. Hodge, S. Rachel, and D. K. Morr, “Implementation of topological quantum gates in magnet-superconductor hybrid structures,” arXiv:2302.04889.